Forecasting methods for occurrence and magnitude of proton storms with solar hard X rays

H. A. Garcia

Space Environment Center, National Oceanic and Atmospheric Administration, Boulder, Colorado, USA

Received 3 October 2003; revised 11 February 2004; accepted 20 February 2004; published 22 June 2004.

[1] A hard X-ray spectrometer (HXRS) was developed jointly by the National Oceanic and Atmospheric Administration (NOAA) Space Environment Center and the Astronomical Institute of the Czech Republic to determine if proton storms could be forecast with greater accuracies than presently available by the existing methods. The HXRS experiment was conceived as a means of proof testing previously discovered empirical relationships between anomalous hard X-ray spectra of hard X-ray flares and solar energetic proton events (SEPs) for space weather forecasting applications. SEPs are showers of highly energetic electrons and ions, mostly protons, that can reach Earth's vicinity within minutes to hours following a moderate to large flare and have the potential of affecting the performance of civilian, military and research satellites as well as certain surface assets. The primary SEP predictor criterion educed during the present study is the requirement that the spectral index, γ, must decline (harden) to at least ≤ 4 for at least 3 min. Flares meeting this criterion have a high association with SEPs. Flares that fail this criterion do not. Other SEP correlative phenomena such as depressed hard X-ray flux and anomalous low temperatures were studied to determine their utility for forecasting purposes. During the study period, March 2000 through December 2002, 107 hard X-ray flares were spectrally analyzed including 16 SEP-associated flares. Fourteen SEP flares were correctly identified, two SEPs were missed, and three false alarms (untrue predictions) were incurred. *INDEX TERMS:* 7514 Solar Physics, Astrophysics, and Astronomy: Energetic particles (2114); 7554 Solar Physics, Astrophysics, and Astronomy: X rays, gamma rays, and neutrinos; 7519 Solar Physics, Astrophysics, and Astronomy: Flares; 7594 Solar Physics, Astrophysics, and Astronomy: Instruments and techniques; *KEYWORDS:* forecasting, proton events, hard X rays

Citation: Garcia, H. A. (2004), Forecasting methods for occurrence and magnitude of proton storms with solar hard X rays, *Space Weather*, *2*, S06003, doi:10.1029/2003SW000035.

1. Introduction

[2] Solar soft X rays constitute the primary observable at the present time for forecasting solar energetic proton (SEP) events [*Balch*, 1999; *Garcia*, 1994; *Garcia and Kiplinger*, 1996; *Garcia et al.*, 1999; *Garcia*, 2004]. However, it was recognized more than 20 years ago, during the Solar Maximum Mission era, that so-called ''gradual hard X-ray bursts'' (GHBs) were also related to SEP events [*Bai*, 1986; *Cliver et al.*, 1986; *Kane and Lin*, 1980]. The latter supposition is reasonable in as much as the majority of particle acceleration occurs during the earliest flare phase when hard X rays predominate and provide the main diagnostic data related to primary energy release. More recent studies have demonstrated that the prime signature relating hard X-ray flares with SEPs is the degree of spectral hardness occurring near flare maximum and in decay [*Garcia*, 1994; *Kiplinger*, 1995; *Garcia and Kiplinger*, 1996]. These latter studies, predicated from the earlier scientific findings, employed hard X-ray spectra from the SMM HXRBS experiment and energetic particle data from ion detectors on GOES 6, GOES 7, and IMP 8 satellites.

[3] Although the present work focused primarily on the robust empirical relationship between anomalously hard spectra and SEPs, it also addressed the thermal and nonthermal aspects of the hard X-ray flare as revealed in the time-dependent spectra. Employing optically thin thermal theory the temperature and emission measure of the thermal portion of the spectrum were extracted in order to investigate possible correlations with the SEP intensity. Similar to soft X rays, it is found that anomalously low temperatures correlate with the SEP intensity. (In soft X rays, anomalously low temperatures correlate with SEP occurrence.) In a separate study the nonthermal part of the hard X-ray spectrum is being investigated to emulate the morphology and microphysics of individual flares, also for possible space weather applications.

[4] These statistical studies provided the empirical basis for the hard X-ray SEP forecasts, but on-orbit verification was needed to demonstrate the utility of this method in a quasi-operational mode, i.e., where, in this special application, the express purpose was to monitor the Sun from exigent space as a proof-of-principle experiment and not for its purely scientific content. In addition to its primary

goal of demonstrating its efficiency in SEP forecasting, the experiment was also intended to test the ability of passive shielding to discriminate between bremsstrahlung radiation coming from the radiation belt environment and true solar radiation.

[5] The present work utilizes and is largely based on the joint NOAA/Czech HXRS experiment aboard the Department of Energy's Multispectral Thermal Imaging (MTI) satellite, launched into a 600 km, Sun-synchronous polar orbit under the auspices of the Department of Defense Space Test Program in March 2000. Although the low polar orbit (incurring frequent night and radiation belt passages) relegated the HXRS to an approximate 33% duty cycle, a representative number of flares have been observed to yield quantitative estimates of SEP prediction efficiency by this method.

[6] The MTI mission which was designed for a 3-year lifetime, encompassing the current solar maximum (occurring on about May 2001), has been extended for at least 2 additional years of operation. The HXRS experiment, however, failed to transmit data after 17 February 2003 despite efforts of the MTI support team to restart the observations and onboard processing.

[7] The paper is organized as follows: Section 2 briefly sketches the general concept of the experiment and lists its principal design goals, attributes, and calibration procedures: preflight, periodic in-flight adjustments, and postlaunch. Section 3 lists the essential qualities required of the hard X-ray data set for spectral analysis. Section 4 describes the tools and methodology used in the analytic process, using two prominent flares as case studies. Section 5 then presents the principal statistical results of the experiment, including a roster of the analyzed SEP flares. Section 6 describes three nonspectral methods for estimating SEP magnitude from hard X-ray spectral data, and section 7 concludes with discussion of the main experimental findings with respect to space weather forecasting.

[8] This paper is the second of two dedicated to SEP prediction. The companion paper [*Garcia*, 2004, hereinafter referred to as Paper I] considered the topic from the standpoint of solar soft X-rays.

2. Instrument Description

[9] The HXRS is designed to measure the hard X-ray spectrum of the Sun in seven energy bands ranging from 13 to 219 keV with 200 ms time resolution. (See Table 1, the last three bands (asterisks) provide total count above the lower energy limit and are not used in spectral analysis.) These logarithmic spaced bins were selected to span the power law configured nonthermal energy range most responsive to SEP occurrence associations, while encompassing the thermal end of the spectrum amenable to temperature and emission measure analysis. Broadbands in each channel were necessary to provide adequate count statistics from a small detector and to accommodate the relatively low spectral resolution (≈25%) of NaI.

[10] The essential instrumental components include a 25 mm NaI crystal, 1.05 mm aluminum prefilter, photomultipler, preamplifier, pulse-height analyzer, and a tunable high voltage (HV) supply. A test of an effective shield against ≥10 keV background radiation is an essential part of this experiment. Two identical scintillation detectors were used to test shielding efficiency: one fully shielded detector encased in organic plastic and equipped with a permanent magnet to deflect boresighted incident electrons, juxtaposed with an unshielded, but otherwise identical, detector. The details of design and construction of the HXRS experiment were presented in three separate meeting venues and appeared in their respective published proceedings [*Farnik et al.*, 1998; *Garcia et al.*, 1998; *Farnik et al.*, 2001].

Table 1. HXRS Energy Bins[a]

Band	From, keV	To, keV
1	12.9	19.0
2	19.0	29.0
3	29.0	44.0
4	44.0	67.2
5	67.2	100.2
6	100.2	147.2
7	147.2	219.5
8*	220	-
9*	250	-
10*	12.6	-

[a]HXRS, hard X-ray spectrometer.

[11] The HXRS was mounted at the sunward end of the spacecraft bus at the centroid of the four-element solar array. This arrangement obviated the need for a special solar pointing platform and provided the HXRS with an unobstructed view of the Sun whenever the host experiment was in standby mode. Data downlinks were made once or twice a day to the Department of Energy (DoE) Sandia receiving station in central New Mexico. Telemetry Data files were then exported to Prague where they were reformatted into SSW-compatible FITS files (SSW is a major software system for processing and analyzing community-wide solar observations [*Freeland and Handy*, 1998]). HXRS data are archived at the Astronomical Institute in Ondrejov, Czech Republic, and on CDs (one CD per month) at SEC in Boulder, Colorado.

2.1. Calibration: Laboratory Preflight, Instrument Inflight

[12] Three forms of calibration were employed: preflight, automated in-flight HV adjustments, and a postlaunch intersatellite comparison.

[13] The preflight calibration consisted of an electronic input-to-output linearity check followed by absolute scale determination of the detector and its electronics employing monoenergetic radioactive sources in order to construct a provisional spectral response matrix for preliminary spectral analysis.

[14] Routine in-flight calibration was invoked to maintain long term stability against aging employing an Am241 pellet on a movable arm that periodically swung into position between the aluminum filter and the crystal detector. The detector response to Am241 was then used in-flight to adjust the HV. To accommodate extreme flares,

Table 2. RHESSI/HXRS Conversions

Band	Energy keV	Conversion Factor
1	13 – 19	7.18
2	19 – 29	4.80
3	29 – 44	1.99
4	44 – 67	2.97
5	67 – 100	1.00
6	100 – 147	4.28
7	147 – 219	5.21

the HV supply was automatically reduced during short periods of high flux rates.

2.2. Calibration: Intersatellite Inflight

[15] Postlaunch HXRS calibration was made possible when directly comparative data could be obtained from a well calibrated solar X-ray satellite. Such data became available from the HESSI (High-Energy Solar Spectroscopic Imager) launched in February 2002 [*Lin et al.*, 2003]. (HESSI was later renamed RHESSI in honor of Reuven Ramaty.) RHESSI is designed to image solar flares from 3 keV (soft X rays) to 20 MeV (gamma rays). The introduction of this exceptional high-energy spectrometer at a time when HXRS was still in operation proved to be an ideal vehicle providing its definitive calibration basis.

[16] Six 2002 flares were found to have good overlap between HXRS and RHESSI. HXRS has fixed energy bins, but RHESSI output may be arbitrarily binned in energy to satisfy the user's particular goals and needs. Therefore seven channels with the same energy edges as HXRS were extracted from RHESSI data for calibration calculations. The transformation coefficients relating the two instruments for moderate to intense flares, M5 to X5 (the range of the overlap flares), were obtained by direct comparision. The HXRS to RHESSI conversion factors are listed in Table 2.

[17] Figure 1 contains precalibration (left) and postcalibration (right) light curves for the 23 July 2002 event showing HXRS(dashed line) photonic flux superimposed on RHESSI (solid line) flux. These data show that the precalibration HXRS fluxes were consistently lower than RHESSI fluxes, particularly in the lowest energies. The spectral plots also revealed that the uncalibrated HXRS fluxes were somewhat irregular and could not always be accurately power law fitted. The result was that the provisional calibrated HXRS measurements tended to give excessively hard spectra by approximately one to two spectral index units in most events. The calibration also had the beneficial effect of further discriminating between SEP and non-SEP flares because the calibrated soft spectra tended to become even softer, whereas harder spectra, such as those associated with SEPs, either did not change materially or softened to a lesser degree.

3. Data Selection

[18] The principal limitations of the HXRS experiment are the limited sensitivity of a small detector, the corrupting effects of the ambient energetic particle background of a low-altitude-high-inclination orbit and outages forced by spacecraft night, and the observing agenda of the host experiment.

[19] Since no universally recognized metric for designating hard X-ray flare importance exists at the present time, it has been convenient in this study to use the NOAA standard metric in soft X rays as a means for establishing a rough equivalence between hard X-ray flux in certain energy bands and the NOAA standard. This procedure, comparing hard X-ray measurements with soft X-ray measurements of the same flare, was employed at several places in this study to help illuminate special physical properties of flares that might not otherwise be evident. Gauging the observability of weak flares by the HXRS was the first of these applications.

[20] Hard X-ray solar emission, at least in the thermal (softer) part of the spectrum, appears to obey an approx-

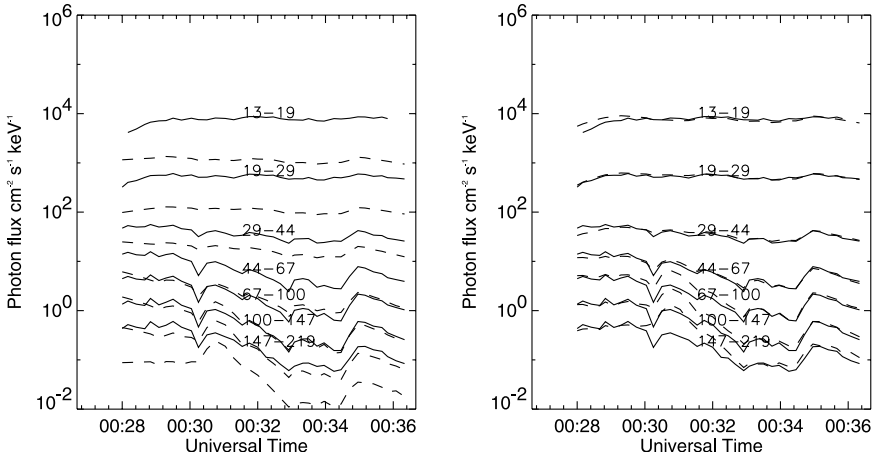

Figure 1. Superimposed light curves from RHESSI (solid line) and HXRS (dashed line) of the July 23, 2002 flare: pre-calibration (left) and post-calibration (right).

imate power law relationship with respect to soft X-rays (see Figure 5); therefore in data selection it was possible to determine beforehand if a certain flare was amenable to spectral analysis with this instrument on the basis of its NOAA class. (The NOAA scheme classifies flares according to a schedule denoted by A, B, C, M, X, where A is the least intense and X the most intense; each lettered class is further subdivided into decimal fractions [*Joint NOAA-USAF Space Environment Services Center*, 1988].

[21] In this system, C-class flares ($1-9 \times 10^{-6}$ W m^{-2}) were below the HXRS threshold. Low level M-class ($1-2 \times 10^{-5}$ W m^{-2}) flares were just above the level of detection, but flares below M1.9 were generally too weak to be spectrally analyzed with confidence.

[22] Discrete localized energetic particle events present the greatest challenge to hard X-ray observations from low-altitude-high-inclination satellite orbits. The MTI orbit period is ≈96 min, including 36 min in Earth shadow. A near-polar inclination incurs four passages through the high latitude radiation belts per orbit and often includes South Atlantic Anomaly (SAA) crossings. Bremsstrahlung radiation from ambient particle populations are frequently an order of magnitude greater than the hard X-ray emission from intense flares (≥X1) and up to two orders of magnitude greater than the weakest flares observable (M1) with this instrument. It was therefore necessary to construct a global geometric radiation belt model, specifically tailored to the HXRS detector response, in order to delineate the HXRS-particularized spatial extent of each belt. An ephemeris computation program was also developed to utilize this model for the prediction of day, night, and radiation belt transits.

[23] The least obtrusive (but still significant) data losses were due to the host experiment's observing schedule which periodically required changing the spacecraft's attitude, directing the HXRS pointing away from the Sun. Additionally, a few important solar events were lost due to mass storage unit overflows or electrical failures of the onboard data processing system.

[24] In terms of available observing time, after the combined effects of night, radiation belt/SAA passages, occasional hiatus caused by the host experiment and other inadvertent data losses have been taken into account, the effective HXRS duty cycle was ∼33%. Moreover, losses due to the low detector threshold that restricted event selection to flares of ≥M1.9, must also be added to the total loss ledger. However, despite these shortcomings, the observation efficiency, expressed in terms of flares analyzed versus flares occurring (Table 3), turned out to be quite comparable to the expected efficiency resulting from the above loss sources during the study period, 12 March 2000 to 31 December 2002.

Table 3. HXRS Observation Efficiency

Year	Occurring	Analyzed	%
2000	79	34	43
2001	142	50	35
2002	109	23	21
Total	330	107	32.4

4. Spectral Analysis

[25] The basic software package for spectrally analyzing hard X-ray flares is contained in the SolarSoft (SSW) suite of programs developed jointly by the NASA GSFC group and the Lockheed-Martin Solar Astrophysics Laboratory at Palo Alto, California [*Freeland and Handy*, 1998]. HXRS data, archived in FITS format, was specifically designed to be SSW compatible which has greatly expedited the task of locating, inspecting, exhibiting, compacting and, finally, extracting a time-dependent series of spectral indices from individual flares. Additionally, the SSW software facilitated the conversion of device-specific count rates into photon fluxes which are needed to extract physical quantities such as thermal temperatures and emission measures. Photon fluxes are also needed to compare the output of differently constructed instruments.

[26] The principal objective of spectral analysis, as it pertains to this experiment, is to evaluate the spectral index γ which quantifies the steepness of a flare's photonic spectrum at discrete times, and to detect variations in its behavior throughout its progress. As previously discussed, unusually hard spectra in a flare is a robust indicator that a SEP may follow. Typically, flare spectra appear to harden near maximum, and then soften during the post-maximum period. With few exceptions this is basically true of all flares; the difference between SEP related and non-SEP related flares is the magnitude that γ attains at near flare maximum, a topic that will be covered in the following sections.

[27] Typically, hard X-ray flare spectra in the HXRS energy range transition from a thermal regime in the vicinity of 10–30 keV to a nonthermal regime above 30 keV with the transition energy varying between 30 and 40 keV. Each regime may be defined by two parameters: temperature and emission measure in the thermal regime and a power law pivot energy and negative index in the nonthermal regime. Spectral analysis consists of parametric fitting and merger of the two energy domains in single, combined solution.

[28] Figure 2 contains spectral plots of two well observed HXRS SEP flares, 24 September 2001 (10:26:10–30) and 23 July 2002 (00:34:57–35:10), exhibiting significantly different spectral behavior. In each event the spectrum has been captured for a short time slice near the flare maximum and employed the same energy interval, 12.9–219 keV. Each plot shows an energy transition from thermal to power law below 40 keV: the September 2001 flare transitioned at about 22 keV and the July 2002 flare at about 32 keV. The tangential curve extensions indicate the spectral fits of the two energy regimes above and below their respective transition energies; the continuous curve shows the merged fit. The plain horizontal bars indicate the observed flux of

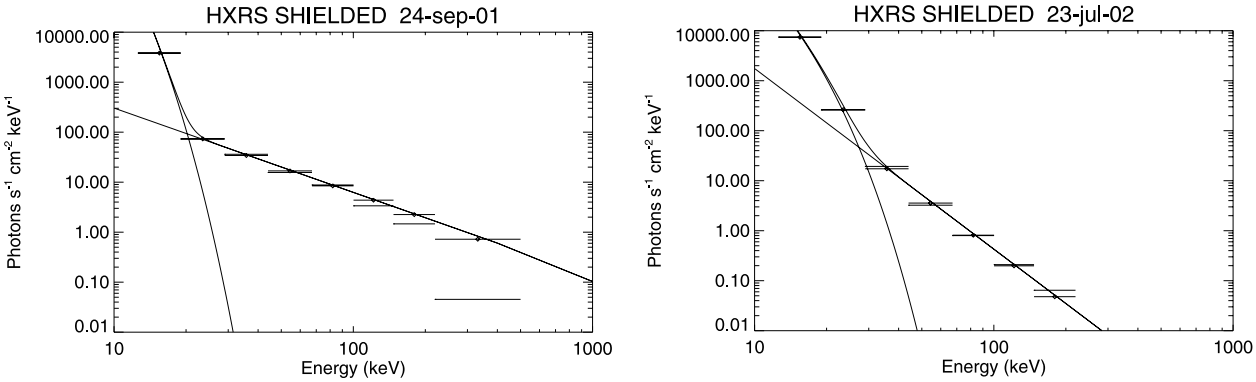

Figure 2. Hard X-ray spectra of two large SEP flares near maximum, (see also Figure 3) showing the merged thermal and non-thermal spectral segments and their theoretically computed extentions. Horizonal bar width indicates the energy band. The highest energy, 219–500 keV, was not included in the spectral fits.

each energy band; the adjacent bars (small center diamond) indicate the corresponding computed flux up to 500 keV. The July 23 flare has also been extensively studied in detail using RHESSI observations [compare *Holman et al.*, 2003, Figure 3].

[29] Figure 3 contains logarithmically scaled light curve plots of all seven HXRS energy bands of the above described flares, juxtaposed with plots of the spectral index time profiles of each event. The latter plot also contains the linearly scaled light curve of one energy (29–44 keV) for temporal comparison. In each of these flares the spectral slopes, γ, vary between 2 and 4, typical of SEP flares.

5. Principal Experimental Results

[30] The principal criterion for SEP prediction deduced from this experiment is that either the spectral index is continuously in the approximate range $2 \leq \gamma \leq 4$, or it hardens to that level one or more times during the main phase of the flare, (even though it may later soften to above that value). Table 4 contains a roster of analyzed

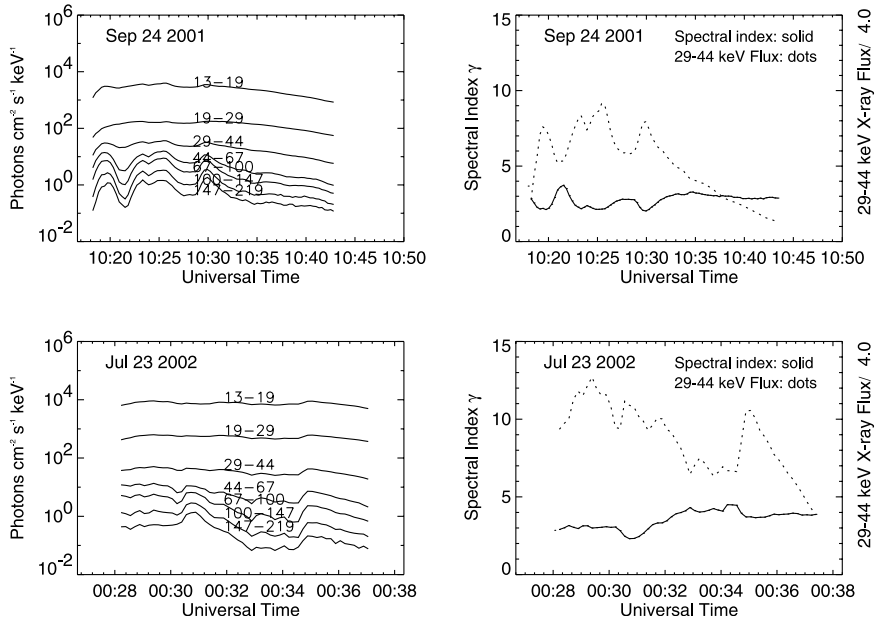

Figure 3. Light curves of seven HXRS energies (left) and spectral index time profiles (solid line) superimposed on the light curve (dotted line) of one energy (right) of the same two flares shown in Figure 2. The linear scales for flux used in the right panel are tended to magnify the small flux variations and show how, in general, they anticorrelate with the spectral index.

16 SEP flares and three non-SEP flares. Only two flares in this group, 8 November and 24 November 2000, showed discernible evidence of continuous hardening in decay. All other SEP flares indicated periods of low γ but not continuous hardening. Therefore in the context of this experiment episodes of continuous hardening are not necessarily required for SEP prediction. The hard-soft-hard spectral evolution typical of the general population of hard X-rays flares is well known and has been previously reported [*Kane and Anderson*, 1970].

[31] No SEP flares observed by HXRS lacked *some* evidence of spectrally hardening in the vicinity of flare maximum; however, two SEP flares, occurring within a short period in 2002 (17 April and 21 April) and originating from the same active region (AR 9906) did not meet the above SEP prediction criterion and thus must be classed as missed predictions. (These peculiar flares, exhibiting other parametric departures from the norm for SEP flares, are discussed further in the following section.) Three non-SEP flares (25 July 2000, 2 September 2001, and 9 September 2001) satisfying the above spectral criterion and lying west of *E*45° must be classified as false alarms (i.e., overpredictions). Eleven analyzed flares without official SEP designations occurred while a previously launched SEP was still active (SEP-in-progress or SIP). Many of the latter exhibited low spectral indices but were reckoned neither as ''hits'' or ''misses.''

[32] The roster of analyzed SEP flares and false alarms are shown in Table 4, listing the average spectral slope γ during the interval of flare maximum; the prediction rank of hit(h), miss (m), or ''false alarm''(f); the magnitude of ensuing SEP event in particle flux units (PFU) at 10 MeV; the NOAA classification of flare importance; and, for comparison, the SEP probability as determined by the soft X-ray low temperature algorithim (Paper I).

Table 4. Observed HXRS SEP Flare Roster[a]

Date	γ	h/m/f	PFU	NOAA	Prob
2000					
Jun 6	2.0	h	84	X2.4	0.63
Jul 14	3.5	h	24000	X5.8	0.79
Jul 25	4.2	f	0	M8.2	0.03
Nov 08	3.5	h	14800	M7.6	0.86
Nov 24	3.5	h	942	X2.1	0.10
2001					
Mar 29	2.5	h	35	X1.8	0.09
Apr 02	4.0	h	1110	X17.	0.86
Sep 24	2.5	h	12900	X2.7	0.55
Oct 22	3.0	h	24	X1.2	0.79
Sep 02	3.5	f	0	M3.1	0.01
Sep 09	3.5	f	0	M9.9	0.03
Nov 17	3.0	h	34	M2.9	0.55
Dec 26	3.0	h	779	M7.2	0.39
Dec 28	2.5	h	76	X3.5	0.55
2002					
Apr 17	5.5	m	24	M2.6	0.19
Apr 21	6.0	m	2520	X1.7	0.77
Jul 23	3.5	h	2000	X4.9	0.14
Aug 22	4.5	h	36	M5.5	0.32
Aug 24	3.5	h	317	X3.3	0.03

[a]SEP, solar energetic proton event; PFU, particle flux unit.

5.1. Summary of HXRS Observations

[33] The overall statisical results of the SEP prediction algorithm based on spectral hardening are summarized in the following inventory: (March 2000–December 2002) (1) 330 occurring flares $\geq$M1, (2) 107 analyzed flares, (3) 16 analyzed SEP flares (45 in period), (4) 14 hits ($\gamma \leq$ 4 for $\geq$3 minutes), (5) 2 misses, (6) 3 ''false alarms,'' and (7) 11 SIPs (SEP-in-progress).

[34] The two primary shortcomings of the spectrally based algorithm, suggested by these results, are the two missed SEPs and the three false alarms. Although this small sample may not seem statistically impressive, it should be noted that these particular events have features in the soft X-ray domain that distinguish them as being different from the majority of flares in their relationship to SEPs.

[35] In the case of the higher-than-normal γ SEP flare, 21 April 2002, the derived soft X-ray probability, 77%, is exceptionally high, indicating that its soft X-ray temperature was exceptionally low. On the other hand, as will be demonstrated in the following section, its hard X-ray thermal temperature was abnormally high. In the case of the three false alarm flares, in each event the soft X-ray probability was near zero, a common feature of non-SEP flares, but an uncommon feature of SEP flares. (The 24 August 2002 SEP flare, occurring near the west limb, also exhibited a low SEP probability in soft X-rays. In most cases involving failed, i.e., ''missed'' soft X-ray predictions, it is often because either the flare was near or over the limb, thus generating a spurious high temperature measurement [*Garcia and McIntosh*, 1992], or the more common phenomenon that large flares naturally trend to higher temperatures [*Garcia*, 1994]).

6. Quantifying Solar Energetic Proton Event Magnitude From Hard X-ray Temperature and Flux

6.1. Temperature and Emission Measure

[36] Hard X-ray spectra of solar flares in the HXRS energy range show evidence of coexistence of thermal-thin target and nonthermal-thick target bremsstrahlung [*Benka*, 1991]. HXRS spans the thermal part of the spectrum in three bands: 13–19, 19–29 and 29–44 keV and the nonthermal spectrum in four bands: 44–67, 67–100, 100–147, 147--219 keV where, in most analyzed flares the transition energy appeared to fall somewhere in the 29–67 keV zone. The thermal (low energy) part may be used to extract plasma temperature and emission measure, whereas the nonthermal (high energy) part may be used to extract certain macrogeometric and certain microphysical components of the current sheet.

[37] As a first step temperature and emission measure are extracted from the lowest energy bands of the thermal spectrum using the thin target equation for bremsstrahlung emissivity [*Mewe et al.*, 1986]. The expression for thin

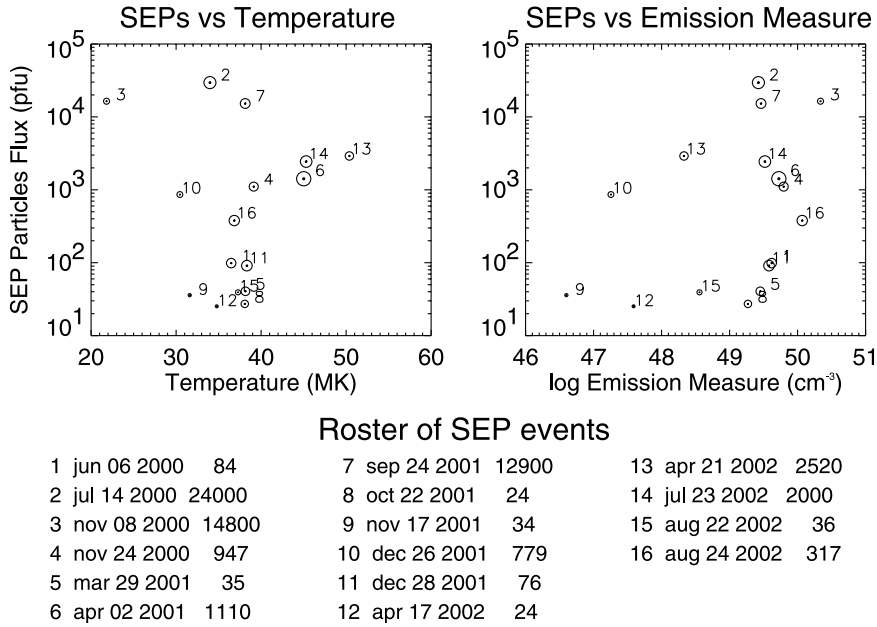

Figure 4. Distribution of SEP event fluxes vs hard X-ray temperatures (left) and emission measures (right). Flare importance are indicated by circles where the diameters are proportional to the logarithm of the peak soft X-ray flux. Except for the three events, Nos. 6, 13 and 14 the SEP magnitude appears to be anticorrelated with X-ray peak flare temperature.

target emissivity involves only the temperature, T and emission measure, Q as free parameters. The solution is non-linear but overdetermined where photon fluxes from three or more energies are invoked simultaneously and converges rapidly when T and Q are initialized with approximate values.

[38] All of the spectrally analyzed HXRS flares, including the 16 SEP flares, were reduced in the above manner to obtain their temperature and emission measures. SEP flux (pfu) in Figure 4 is plotted separately against temperature (left panel) and emission measure (right panel). The SEP flare roster listed below Figure 4 references the chronologically ordered serial number of each flare to the numbered symbols shown in Figure 4 and includes the date and pfu of each associated SEP event. These flare designations are also used in Figures 5, 6, and 7 to key each parametric datum to its respective event date.

[39] The most noteworthy feature in the temperature plot, Figure 4 (left), is that all but three SEP flares fall into the low temperature regime below 40 MK. Moreover, the majority of high temperature flares ($\geq$40 MK) were non-SEP (not shown) M-class flares. The three highest temperature SEP flares are peculiar in some respect (although not the same respect). It may be recalled, the April 21, 2002 (#13), was a miss because of its relatively large γ; April 2, 2001 (#6) was an extreme soft x-ray flare but its soft X-ray temperature was exceptionally low at that level of intensity; July 23, 2002 (#14) was also an extreme soft x-ray flare but was relatively weak in hard X-rays as will be discussed below. It may also be significant that the lowest temperature SEP flare, November 8, 2000 (#3) (T = 21.4 MK) was also among the largest SEP events on record.

[40] The emission measure plot, Figure 4 (right) reveals no outstanding SEP signature and shows, as expected, that emission measure of the hard X-ray flare increases roughly in proportion to the flare's importance, the extreme low temperature 8 November 2000 flare being the main exception.

6.2. Depressed Hard X-ray Flux

[41] It is reasonable to expect that, in general, a hard X-ray flare's peak flux, Φ_{HXR}, should increase in proportion to the flare's soft X-ray's peak flux, Φ_{SXR}. This is certainly true of the majority of flares which are not associated with SEPs. Figure 5 is constructed to demonstrate simultaneously the relationship existing between hard and soft X-rays in a sample flare population, as well as the correlation between SEP magnitude and hard X-ray flux in lowest four HXRS energy bins. To quantify the latter correlation SEP magnitudes are depicted as circles proportional to logarithmic pfu. (Note that the non-SEP, quasi-linear log-log distributions (crosses) connote a near power law relationship, as previously noted.)

[42] It is also evident from these data that SEP flares appear to depart from the general distribution of non-SEP flares and exhibit depressed flux levels in these channels. To emphasize the latter point the non-SEP and SEP flare logarithmic flux distributions were fit quadratically: solid line curves for non-SEP flares and dashed curves for SEP flares. This phenomenon appears

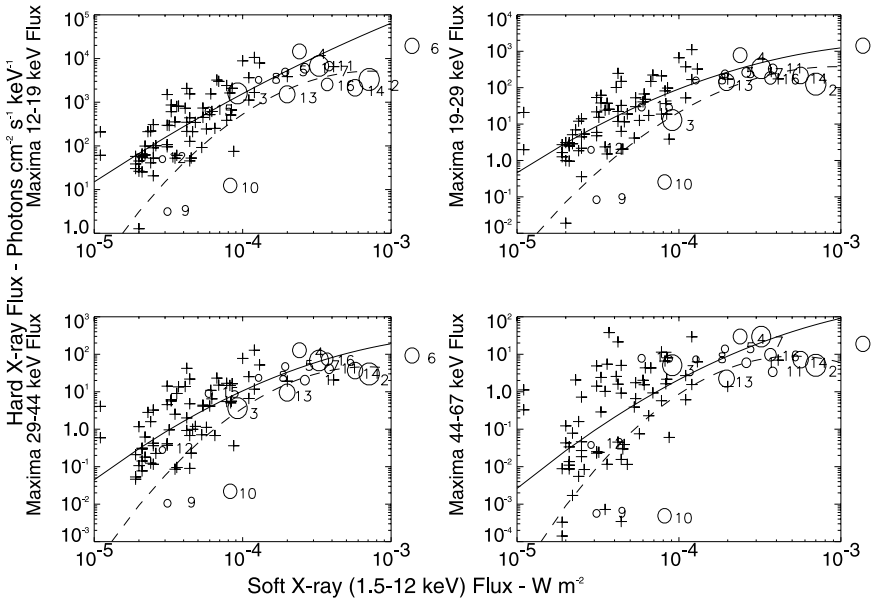

Figure 5. Distribution of hard X-ray flux in four energy bins vs soft X-ray flux. Non-SEP(solid line) and SEP flare (dashed line) distributions are fitted with quadratics. Circle diameters are proportional to log SEP magnitude.

to hold only for the thermal regime and fails in the nonthermal regime.

6.3. Temperature and Normalized Hard X-ray Flux

[43] Despite the tendency of low temperature and depressed hard X-ray fluxes in flares to correlate with SEP magnitudes as demonstrated in Figures 4 and 5, neither association is sufficient in itself to provide an unambiguous indicator of SEP magnitude. However since in each association the observed parameter trends to lower values with increasing SEP magnitude, it may follow that the product of the two parameters, i.e.,

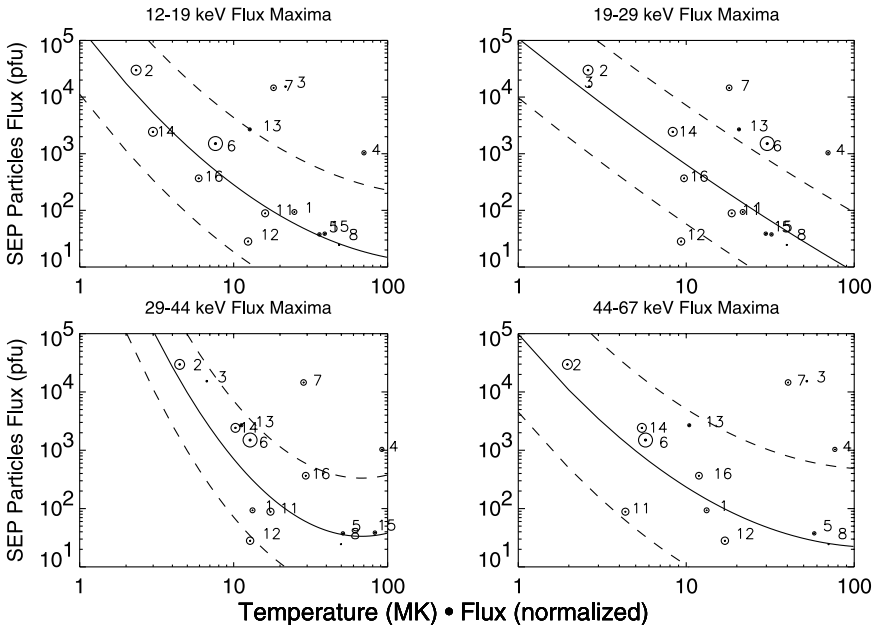

Figure 6. Particle flux from SEP events are plotted directly against the product $T \times \Phi_{Nor}$ (in the range of 1 to 100) for the same energy bands shown in Figure 5. Main least squares fit indicated by solid line; $\geq 1\sigma$ limits by dashed lines. Similar to Figure 4, the diameters of the individual plot point circles are proportional to the logarithm of the peak soft X-ray flux to show the influence (if any) of each flare's importance in this relationship.

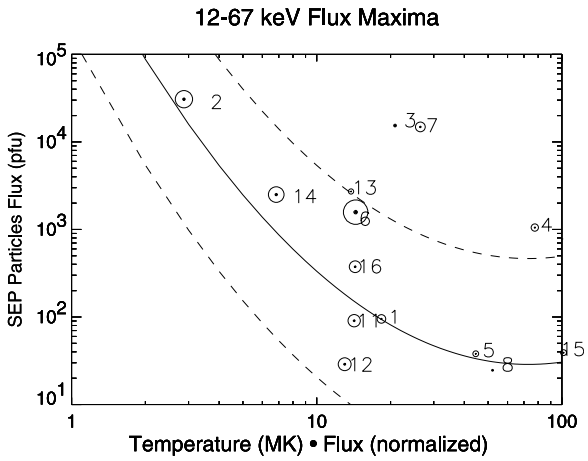

Figure 7. Results of combining all four hard X-ray passbands (12–67 keV) of all SEP events into a single solution. The solid and dashed curves have the same meaning as in Figure 6. The circle diameters are again proportional to flare importance.

$T \times \Phi_{HXR}$, may provide a more robust indicator than either by itself.

[44] Moreover, as expected and as Figure 5 graphically demonstrates, hard X-ray flux increases with the flare's importance as depicted in soft X-rays. It is necessary, therefore, to normalize the flux in each energy band in order to remove this bias. Normalized hard X-ray fluxes, Φ_{Nor}, are computed by dividing each observed flux by its averaged value (indicated by the solid line in Figure 5) from the distribution of non-SEP hard X-ray peak fluxes in each passband versus peak soft X-ray fluxes. The quadratic logarithmic fit coefficients for hard X-ray versus soft X-ray are given in equation (1) and Table 5.

$$\log \Phi_{HXR} = C_0 + C_1 \times \log \Phi_{SXR} + C_2 \times (\log \Phi_{SXR})^2 \qquad (1)$$

where Φ_{HXR} = hard X-ray flux (photons cm^{-2} s^{-1} keV^{-1}) Φ_{SXR} = soft X-ray flux (W m^{-2}).

[45] Figure 6 compares the particle flux of the HXRS associated SEP events with their respective temperature-normalized flux products. These scatterplots employ the same energy bands as in Figure 5; however, in this case the SEP magnitude is plotted directly against the product $T \times \Phi_{Nor}$. The principal concentrations of the data points appear to be arranged approximately along a diagonal that extends from the upper left corner where the largest particle fluxes correlate with the smallest $T \times \Phi_{Nor}$, to the lower right corner where the smallest particle fluxes correlate with the largest $T \times \Phi_{Nor}$. Quadratic fits to the logarithmic form of these data are indicated by solid lines in each energy band; the 1 standard deviation limits of these dispersions are indicated by dashed lines. Significant off diagonal scatter persists at all energy bands where the persistent largest outliers (>1σ) consisted of mainly three events: 8 November 2000; 24 November 2000 (the only two continuous hardening flares in the sample); and 24 September 2001.

Table 5. Non-SEP Hard X-ray Versus Soft X-ray

	Quadratic Fit Coefficients		
Passband, keV	C_0	C_1	C_2
13–19	7.621	0.404	−0.176
19–29	−0.029	−2.71	−0.553
29–44	−0.222	−2.43	−0.531
44–67	−1.107	−2.99	−0.657

[46] In order to quantify and consolidate the above findings these data were processed collectively as shown in Figure 7. After averaging the products $T \times \Phi_{Nor}$ from all four hard X-ray passbands and combining these results into a single-solution SEP magnitude, Φ_{SEP} may be expressed quantitatively by the empirical function,

$$\log \Phi_{SEP} = 5.147 - 3.442 \log(T \times \Phi_{Nor}) + 0.877(\log(T \times \Phi_{Nor}))^2 \qquad (2)$$

where Φ_{SEP} = SEP flux (pfu), T = SEP flare temperature (MK), and Φ_{Nor} = normalized hard x-ray flux (unitless).

7. Summary and Conclusions

[47] Interplanetary energetic particle events frequently associate with an uncommon species of solar flare characterized by unusually hard spectra when observed in hard X-rays. The HXRS space flight experiment was designed and flown to determine if this heuristic relationship is sufficiently robust to warrant the development of a solar hard X-ray spectrometer for operational use aboard geosynchronous, Sun-monitoring satellites such as GOES. This experiment was also intended to test the efficiency of organic plastics and deflection magnets to shield detectors in the hard X-ray spectrum 10–200 keV against energetic electron populations in the cusp of the radiation belts (representative of conditions at geosynchronous, equatorial, orbit).

[48] Only those events that could be spectrally analyzed with relative confidence are reported. This constraint winnowed the crop of candidate events from an original 330–107. In rough correspondence, 16 SEP flares were analyzed out of an original 45 occurring. Of this set, 14 SEPs were correctly identified, two were missed and three were false. Table 6 compares these results against previously reported studies, also dedicated to SEP forecasting.

Table 6. SEP Prediction Contingencies

	Observed	Not observed
	Garcia	
Predicted	14	3
Not predicted	2	87
	Heckman	
Predicted	17	16
Not predicted	4	63
	Kiplinger	
Predicted	22	8
Not predicted	1	700

[49] The middle panel results are from *Heckman et al.* [1992]. The lower panel results are from *Kiplinger* [1995] who also employed hard X-ray flare spectra. Kiplinger obtained his data from the SMM HXRBS experiment 1980–1989; used different data selection criteria; covered a period at least three times longer than the present study; was able to analyze much weaker flares; and therefore encompassed a data set almost an order of magnitude larger than the present study.

[50] The current results of the present study are somewhat comparable with Heckman with respect to hits, misses, and true rejections (lower right in each 2×2 box) but are substantially better with respect to false alarms. The Kiplinger results also appear to be comparable with respect to hits and misses but less so with respect to false alarms.

[51] The principal objective, to test whether energetic proton storms, SEPs, could be forecast in advance of the event by real-time hard X-ray observations, was, in principle, investigated by this experiment even though severely constrained by a number of inhibiting factors discussed in section 3. Two leading factors affect the time-of-arrival of energetic particles at Earth: the location (principally the Central Meridian Distance or CMD) of the active regions (AR) and the highest energy particles that are acclerated during the event. Well connected particles arise from ARs in the range of W10 to W90 CMD. Well-connected 10 MeV protons ($v = 4.38 \times 10^7$ ms^{-1}) can arrive at Earth in $\sim$1 hour; well-connected 100 MeV protons ($v = 1.38 \times 10^8$ ms^{-1}) arrive in $\sim$20 min. However, 100 MeV protons that are not well connected are rarely observed (J. Kunches private communication, 2003).

[52] At the present time, no operational satellite conducts hard X-ray observations of the Sun dedicated to SEP forecasting; therefore no operational methods have been developed for this purpose. Estimates of times required to reduce individual events must be based on experience using historical data, factoring in the inevitable procedural improvements attending any operational scenario: I suggest that the operation could consume 10 minutes, allowing about 10 minutes of warning for even the most energetic and well connected events.

[53] Referring to the short window available to the forecaster when GeV energy particle fluxes are directed toward the Earth, Paper I discussed the ''insurmountable problem affecting all SEP forecasting schemes.'' The method described herein is intended to enhance forecasting outcomes for the general case and is thus subject to the same shortcomings in this regard as all other SEP predictive schemes.

[54] **Acknowledgments.** HXRS was designed and built by the private firm Space Devices in Prague, Czech Republic and funded primarily by the NOAA Office of International Affairs' Joint Fund and the Czech Academy of Science. Additional funding was obtained from the NASA Space Radiation Analysis Group (SRAG) and the Air Force European Office of Aerospace Research and Development (EOARD). Space Flight was provided by the Department of Energy Multispectral Thermal Imaging (MTI) project. Spacecraft integration, launch, and the first year of on-orbit operation was financed by the Department of Defense Space Test Program.

References

Bai, T. (1986), Two Classes of Gamma-ray Proton Flares: Impulsive and gradual, *Astrophys. J.*, *308*, 912.

Balch, C. (1999), SEC Proton prediction model: Verification and analysis, *Radiation Measurements*, vol. 30, edited by E. V. Benton and G. D. Badhwar, pp. 231–250, NASA, Greenbelt, Md.

Benka, S. G. (1991), A Thermal/nonthermal Approach to Solar Flares, *NASA Tech.*, *4323*.

Cliver, E. W., B. R. Dennis, A. L. Kiplinger, S. Kane, D. F. Neidig, N. Sheeley, and M. Koomen (1986), Solar gradual hard X-ray bursts: Obervations and an interpretation, *Adv. Space Res.*, *6*(6), 249.

Farnik, F., H. Garcia, and A. L. Kiplinger (1998), Solar broad-band hard X-ray spectrometer onboard the MTI satellite, in *A Crossroads for European Solar and Heliospheric Physics, Tenerife*, Spec. Publ. 417. Eur. Space Agency, Paris.

Farnik, F., H. Garcia, and M. Karlicky (2001), New solar broad-band hard X-ray spectrometer: First results, *Sol. Phys.*, *201*, 357.

Freeland, S. L., and B. N. Handy (1998), Data analysis with the SolarSoft system, *Sol. Phys.*, *182*, 497.

Garcia, H. A. (1994), Temperature and hard X-ray signatures for energetic proton events, *Astrophys. J.*, *420*, 422.

Garcia H. A. (2004), Forecasting methods for occurrence and magnitude of proton storms with solar soft X rays, *Space Weather*, *2*, S02002, doi:10.1029/2003SW000001.

Garcia, H. A., and A. L. Kiplinger (1996), Low temperature soft X-ray flares, spectrally hardening hard X-ray flares and energetic interplanetary protons, in *Solar Drivers of Interplanetary and Terrestrial Disturbances*, *ASP Conf. Ser.*, vol. 95, edited by K. Balasubramaniam, S. Keil, and R. Smartt, Astron. Soc. of the Pac., San Francisco, Calif.

Garcia, H., and P. S. McIntosh (1992), High temperature flares observed in broadband soft X-rays, *Sol. Phys.*, *141*, 109.

Garcia, H. A., F. Farnik, and A. L. Kiplinger (1998), Hard X-ray spectroscopy for proton flare prediction, *Missions to the Sun II, SPIE Conf.*, vol. 3442, Int. Soc. for Opt. Eng., Bellingham, Wash.

Garcia, H. A., S. Greer, and R. Viereck (1999), Prediction solar energetic particle events from flare temperatures, in *Magnetic Fields and Solar Processes*, *Proc. 9th European Meeting on Solar Phys.*, Spec. Publ. 448, Eur. Space Agency, Paris.

Heckman, G. R., J. M. Kunches, and J. H. Allen (1992), Prediction and evaluation of solar particle events based on precursor information, *Adv. Space Res.*, *12*(2-3), 313.

Holman, G. D., L. Sui, R. A. Schwartz, and G. Emslie (2003), Electron bremsstrahlung hard X-ray spectra, electron distributions, and energetics in the 2002 July 23 solar flare, *Astrophys. J.*, *595*, 97.

Joint NOAA-USAF Space Environment Services Center (1988), *SESC Glossary of Solar-Terrestrial Terms*, U.S. Govt. Print. Off., Washington, D. C.

Kane, S., and K. A. Anderson (1970), Spectral characteristics of impulsive solar flare X-rays $\geq$10 keV, *Astrophys. J.*, *162*, 1003.

Kane, S., and R. Lin (1980), Prediction of solar events using hard X-ray emission, *Solar-Terrestrial Prediction Proceedings*, vol. III, *Sol. Act. Pred.*, edited by R. F. Donnelly, NOAA, Boulder, Colo.

Kiplinger, A. (1995), Comparative studies of hard X-ray spectral evolution in solar flares with high energy proton events observed at Earth, *Astrophys. J.*, *453*, 973.

Lin, R. P., et al. (2003), RHESSI observations of particle acceleration and energy release in an intense solar gamma line flare, *Astrophys. J.*, *595*, 69.

Mewe, R., J. Lemen, and G. van den Oord (1986), Calculated X-radiation from optically thin plasmas, *Astro. Astrophys.*, *65*, 511.

H. A. Garcia, Space Environment Center, National Oceanic and Atmospheric Administration, 325 Broadway, Boulder, CO 80305, USA. (howard.a.garcia@noaa.gov)